REGULAR PAPER

High-Precision Tracking Control of a Piezoelectric Micro-nano Platform Using Sliding Mode Control with the Fractional-Order Operator

Rui Xu[1] · Wei Pan[2] · Zhongshi Wang[1] · Dapeng Tian[1]

Abstract

In this paper, a sliding mode control using a fractional-order operator (SMCFO) method is presented for the hysteresis of a piezoelectric (PZT) micro-nano platform. At first, the hysteresis of the PZT micro-nano platform is described using the Duhem model. With respect to the sliding mode controller design, we introduce a fractional-order operator into the design of the sliding mode surface and enhance the performance of the proposed controller. The nonlinear switching action of the controller is eliminated through a smooth control action by applying an uncertainty and disturbance estimation technique. The stability of the proposed controller is analyzed using the Lyapunov theorem. Simulations and experimental results demonstrate that the SMCFO method achieves a no-load high precision tracking control of the PZT micro-nano platform and is also robust against load perturbations of the platform.

Keywords Sliding mode control · Fractional calculus · Tracking control · Hysteresis · Piezoelectric

1 Introduction

A piezoelectric (PZT) micro-nano platform, with its high stiffness, large output force, and fast response, has been the core component in a variety of the micromachining and nanomanipulation fields, such as atomic force microscopes [1], ultraprecision machining equipment [2], and scanning tunneling microscopy [3]. However, the hysteresis nonlinearity induced by PZT materials makes it significantly difficult to achieve high-precision tracking positioning control of the PZT micro-nano platform. To describe

this hysteresis nonlinearity, some operator-based hysteresis models have been developed, including the Preisach [4, 5], Prandtl–Ishlinskii (PI) [6], and Krasnosel' skii–Pokrovskii (KP) models [7, 8], etc. For example, the KP model based on the Elman neural network captures the hysteresis of the magnetically controlled shape memory alloy actuator [9]. However, a large number of hysteresis operators are superimposed to ensure modeling accuracy leading to a complex hysteresis model and controller. Thus, the differential-equation-based hysteresis models (such as the Bouc–Wen [10, 11], Backlash-like [12], and Duhem models [13]) have been studied. As an example, the Bouc–Wen model, identified by the bat-inspired algorithm, is used to capture the hysteresis of a PZT positioning stage, the experimental results of which verify its effectiveness [14].

Based on such hysteresis models, some feedforward compensation control schemes have been proposed to mitigate the hysteresis of the PZT platform. For example, an inverse compensation control approach based on the inverse PI or KP model was adopted to compensate the hysteresis nonlinearity of the PZT actuators or stages [7, 15]. Owing to its dependence on modeling accuracy, some feedback closed-loop control techniques, such as iterative learning control [16], model predictive control [17–19], model reference control [20], and repetitive control [21, 22], have been investigated to deal with the hysteresis nonlinearity of

✉ Dapeng Tian
d.tian@ciomp.ac.cn

Rui Xu
xur@ciomp.ac.cn

Wei Pan
panwei17@mails.jlu.edu.cn

Zhongshi Wang
zhongshiwang@ciomp.ac.cn

1 Key Laboratory of Airborne Optical Imaging and Measurement, Changchun Institute of Optics, Fine Mechanics and Physics, Chinese Academy of Sciences, Changchun 130033, China

2 Department of Control Science and Engineering, Jilin University, Changchun 130022, China

the PZT micro-nano platform. Based on an overview of the existing control strategies, the robustness and accuracy of these control methods are the major problems. Hence, this study focuses on the tracking controller of a PZT micro-nano platform with different loads. Note that sliding mode control is a frequently used nonlinear control method owing to its insensitivity to disturbances [23–25]. It drives the system states onto the sliding mode surface and keeps it moving along the sliding mode surface. Once the states of the systems reach the sliding mode surface, the controller is robust toward modeling uncertainties and exterior disturbances. In this study, we employ these advantages of the sliding mode control to design a new sliding mode controller achieving a highly accurate tracking control of the PZT micro-nano platform. Unlike the existing sliding mode surface, a fractional-order operator is introduced into the design of the sliding surface to obtain additional degrees of freedom, which further improves the performance of the sliding mode control. However, the most noticeable that the chattering problem of the sliding mode control is an unavoidable issue. A boundary layer approach [26], a filtering method [27], and a high-order sliding mode technique [28, 29] have been used to solve the chattering phenomenon of a sliding mode controller. Moreover, sliding mode control and a perturbation estimation method have been combined together in existing literature [30]. For instance, a sliding mode controller based on an uncertainty and perturbation estimation technique was reported [31], and a controller was applied to a class of nonlinear systems, the simulation results show the its effectiveness. Nevertheless, it remains to be seen whether this method can be applicable to a practical system.

This study utilizes the Duhem model to describe the PZT micro-nano platform system. To achieve high-precision tracking control for the platform, we propose a new SMCFO scheme based on the fractional-order operator. Instead of using the signum function as the robust term of the controller, the uncertainty and perturbation estimation approach is applied, essentially achieving the advantage of a chattering-free state. The Lyapunov stability theorem proves the stability of the proposed control approach in theory. A series of trajectory tracking experiments with some different loads were implemented to validate the performance of the proposed controller. Experimental results show that the SMCFO method achieves a significant robustness and high tracking accuracy.

The remainder of this paper is organized as follows. The Duhem model is introduced in Sect. 2. Next, the design of the SMCFO scheme is outlined and its stability is analyzed in Sect. 3. Results of simulations and experiments are discussed in Sect. 4. Finally, some concluding remarks are presented in Sect. 5.

2 System Description of the Piezoelectric Micro-nano Platform

The Duhem model was proposed for the hysteresis modeling by P. Duhem in 1987, and it was expressed using a differential equation involving the output, input and the change rate of the input. As reported in literature [32, 33], the Duhem model has been widely utilized in hysteresis nonlinearity modeling and the compensation of smart material driven systems owing to its simple model structure and the advantage of easy identification of model parameters. In addition, it can capture hysteresis in various forms related to a different input driven signal, which is suited to the modeling of a PZT micro-nano platform. In this study, we use the Duhem model to describe the hysteresis nonlinearity of the PZT micro-nano platform, and the mathematical formula of which is expressed as follows:

$$\begin{cases} \dot{x}(t) = a_0 x(t) + a_1 u(t) + a_2 \psi(t) + \phi(t) \\ \dot{\psi}(t) = \alpha |\dot{u}(t)| \big[f(u(t)) - \psi(t) \big] + \dot{u}(t) g(u(t)) \\ y(t) = x(t), \end{cases} \tag{1}$$

where $u(t)$, $y(t)$, and $\psi(t)$ are the input driven signal, output displacement, and hysteresis state of the PZT micro-nano platform, respectively; $\dot{\psi}(t)$ is the derivative of $\psi(t)$ with respect to time t, which is described by the second equation in formula (1); and $\phi(t)$ is the total disturbance, which includes the parameter uncertainty term, external interference, and external loading. In addition, a_0, a_1, and a_2 represent the nominal parameters, which are positive numbers; both $f(u(t))$ and $g(u(t))$ are the piecewise continuous function. Let $\Omega[a, b]$ be continuous function sets on the closed interval $[a, b]$ and $f(x) \in \Omega[a, b]$. With respect to any given $\varepsilon > 0$, there is a polynomial sequence $\{p(x)\}$ with respect to $x\epsilon[a, b]$ such that

$$\max_{a \leq x \leq b} |f(x) - p(x)| < \varepsilon, \tag{2}$$

where the polynomial sequence $\{p(x)\}$, uniformly approximate to the continuous function $f(x)$, is then written as follows:

$$f(x) \cong p(x) = p_0 + p_1 x + p_2 x^2 + \cdots + p_c x^c. \tag{3}$$

Here c is the order of the function $p(x)$.

The continuous functions $f(u(t))$ and $g(u(t))$ belonging to $\Omega[a, b]$ can be obtained by the following polynomial approximation:

$$\begin{cases} f(u(t)) \cong f_0 + f_1 u(t) + \cdots f_p u^p(t) = \sum_{i=0}^{p} f_i u^i(t) \\ g(u(t)) \cong g_0 + g_1 u(t) + \cdots g_q u^q(t) = \sum_{j=0}^{q} g_j u^j(t), \end{cases} \tag{4}$$

where p and q are the orders of $f(u(t))$ and $g(u(t))$, respectively. In addition, f_i and g_j are constants. The Duhem model of the PZT micro-nano platform is rewritten as follows:

$$\begin{cases} \dot{x}(t) = a_0 x(t) + a_1 u(t) + a_2 \psi(t) + \phi(t) \\ \dot{\psi}(t) = \alpha |\dot{u}(t)| \left(\sum_{i=0}^{p} f_i u^i(t) - \psi(t) \right) \\ \qquad\quad + \dot{u}(t) \sum_{j=0}^{q} g_j u^j(t) \\ y(t) = x(t). \end{cases} \tag{5}$$

To obtain the unknown parameters of the Duhem model, we first have to determine its order. The higher orders of the model are associated with higher modeling accuracy. However, a higher order model needs more computations. In this study, the interior point method is used to identify the unknown parameters by minimizing the sum of the errors between the actual output of the PZT micro-nano platform and the output of the Duhem model. The orders of the Duhem model are determined using a trial and error method. The experimental results are shown in Table 1. From Table 1, it is evident that the root-mean-square error (RMSE) and the maximum error (MAXE) rate decrease with an increase in the model orders. To balance the identification computation with the modeling accuracy, the orders of the Duhem model are set as $p = 3$ and $q = 2$. The obtained parameters of the Duhem model are shown in Table 2. The hysteresis curves produced by the PZT micro-nano platform and the estimated error of the Duhem model are shown in Fig. 1.

Table 1 Parameter identification results of the Duhem model with different orders

p	q	RMSE (µm)	MAXE Rate (%)
1	1	0.2363	1.26
1	2	0.2362	1.25
1	3	0.2357	1.24
2	1	0.1051	0.85
2	2	0.0988	0.82
3	1	0.0876	0.78
3	2	0.0761	0.69

Table 2 Parameters of the Duhem model for the PZT micro-nano platform

Parameters	Values	Parameters	Values
a_0	− 1550.36	f_2	0.1538
a_1	1501.87	f_3	−0.0118
a_2	− 1643.54	g_0	−0.0309
f_0	0.9704	g_1	0.0421
f_1	− 0.9206	g_2	−0.0038
α	0.3602	–	–

3 Sliding Mode Controller Design Based on the Fractional-Order Operator

In this section, we proposed a novel sliding mode controller to achieve high-precision tracking control of the PZT micro-nano platform. At first, to design the SMCFO method, the tracking error is defined as follows:

$$e(t) = x_d(t) - x(t), \tag{6}$$

where $x_d(t)$ is the desired trajectory signal, and $x(t)$ is the actual output displacement of the PZT micro-nano platform.
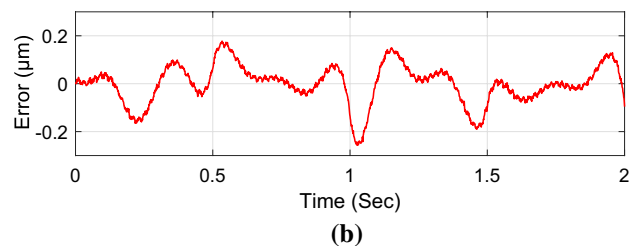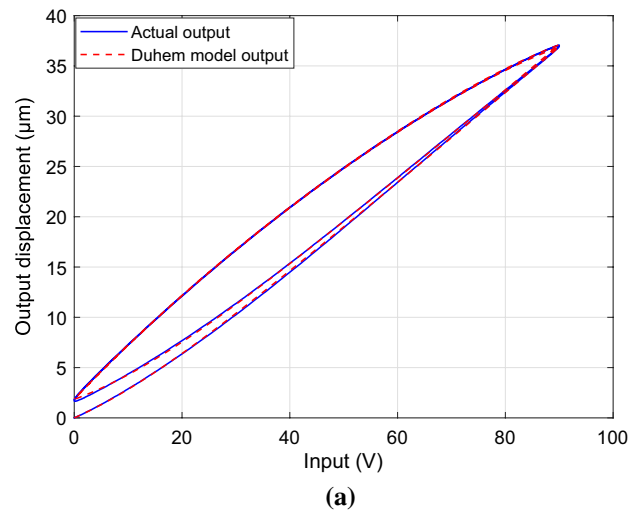

Fig. 1 Hysteresis loop and error produced by the PZT platform and Duhem model. **a** Hysteresis loop. **b** Modeling error curve

Based on the tracking error, we define a fractional-order sliding mode surface as follows:

$$\zeta(t) = e(t) + \lambda(_0D_t^r e(t)), \tag{7}$$

where λ is a positive constant. In addition, $_0D_t^r(\cdot)$ represents the fractional-order operator, and r satisfies $0 < r < 1$. In this study, we use the caputo fractional derivative to complete the fractional-order operation, which is defined as follows:

$$_{t_0}D_t^r f(\cdot) = \begin{cases} \frac{1}{\Gamma(m-r)} \int_0^t \frac{f^{(m)}(\tau)}{(t-\tau)^{r-m+1}} d\tau, & m-1 < r < m, \\ \frac{d^m}{dt^m} f(t), & r = m, \end{cases} \tag{8}$$

where m is the first integer larger than r.

Next, taking the time derivative of (7), the dynamic sliding mode surface is as follows:

$$\begin{aligned} \dot{\zeta}(t) &= \dot{e}(t) + \lambda(_0D_t^r \dot{e}(t)) \\ &= (\dot{x}_d(t) - \dot{x}(t)) + \lambda(_0D_t^{r+1} e(t)). \end{aligned} \tag{9}$$

Combined with (5), (9) is written as follows:

$$\begin{aligned} \dot{\zeta}(t) &= \dot{x}_d(t) - a_0 x(t) - a_1 u(t) - a_2 \psi(t) - \phi(t) \\ &\quad + \lambda(_0D_t^{r+1} e(t)). \end{aligned} \tag{10}$$

With the assignment of $\dot{\zeta}(t) = 0$ and without regard to the total disturbance $\phi(t)$, an equivalent sliding mode control law is obtained as follows:

$$u_{eq}(t) = \frac{1}{a_1}[\dot{x}_d(t) - a_0 x(t) - a_2 \psi(t) + \lambda(_0D_t^{r+1} e(t))]. \tag{11}$$

To eliminate the total disturbance of the PZT micro-nano platform, we design a robust control term to keep the states moving on the sliding mode surface according to the Lasalle invariance principle. The robust control law is then proposed as follows:

$$u_r(t) = -\frac{1}{a_1}[\hat{\phi}(t) - \eta\zeta(t)], \tag{12}$$

where $\hat{\phi}(t)$ is the estimated value of the total disturbance $\phi(t)$, and η is a positive constant.

Then, combining (11) and (12), the total control law is

$$u(t) = u_{eq}(t) + u_r(t). \tag{13}$$

With regard to the total disturbance $\phi(t)$, we introduce the total control law $u(t)$ into (10), which is derived as follows:

$$\dot{\zeta}(t) = \hat{\phi}(t) - \phi(t) - \eta\zeta(t). \tag{14}$$

According to (14), $\phi(t)$ and its estimated value $\hat{\phi}(t)$ are unknown. Then, an uncertainty estimation method is designed based on a low-pass filter $G_{lf}(s)$. At first, (14) is rewritten as follows:

$$\phi(t) = \hat{\phi}(t) - \eta\zeta(t) - \dot{\zeta}(t). \tag{15}$$

Combined with (15) and the designed method for the low-pass filter, the estimated value of the total disturbance $\hat{\phi}(t)$ is obtained as follows:

$$\begin{aligned} \hat{\phi}(t) &= g_{lf}(t) * \phi(t) \\ &= g_{lf}(t) * [\hat{\phi}(t) - \eta\zeta(t) - \dot{\zeta}(t)], \end{aligned} \tag{16}$$

where $g_{lf}(t) = L^{-1}\{G_{lf}(s)\}$ represents the impulse response function of the $G_{lf}(s)$; $L^{-1}\{\cdot\}$ is the inverse Laplace transformation, and $*$ represents the convolution operation.

According to (16), $\phi(t)$ is replaced by $\hat{\phi}(t)$ and yields the following:

$$\hat{\phi}(t) = [-\eta\zeta(t) - \dot{\zeta}(t)] * \frac{g_{lf}(t)}{1 - g_{lf}(t)}. \tag{17}$$

Then, we design the low-pass filter in the following form:

$$G_{lf}(s) = \frac{1}{\tau_{lf}s + 1}, \tag{18}$$

where the τ_{lf} is a positive constant. Based on (18), take the Laplace transform of (17), which is obtained as follows:

$$\hat{\phi}(s) = \frac{1}{\tau_{lf}s}[-\eta\zeta(t) - \dot{\zeta}(t)]. \tag{19}$$

Taking the inverse Laplace transform of (19), we then obtain

$$\hat{\phi}(t) = \frac{1}{\tau_{lf}}\left[-\eta\int_0^t \zeta(\tau)d\tau - \zeta(t)\right]. \tag{20}$$

Therefore, the robust control law term is shown as follows:

$$\begin{aligned} u_r(t) &= -\frac{1}{a_1}\left[\frac{1}{\tau_{lf}}(-\eta\int_0^t \zeta(\tau)d\tau - \zeta(t))\right] \\ &= \frac{\eta}{a_1\tau_{lf}}\int_0^t \zeta(\tau)d\tau + \frac{1}{a_1\tau_{lf}}\zeta(t). \end{aligned} \tag{21}$$

Theorem *Consider the system* (1) *of the PZT micro-nano platform with the total disturbance* $\phi(t)$. *Using the control law* (22), *there exist constants* η, r, τ_{lf}, *and* λ *such that the proposed SMCFO method, shown in Fig.* 2, *is stable and allows the output of the PZT micro-nano platform to accurately track the desired trajectory signal.*

$$\begin{aligned} u(t) &= \frac{1}{a_1}[\dot{x}_d(t) - a_0 x(t) - a_2 \psi(t) + \lambda(_0D_t^{r+1} e(t))] \\ &\quad + \frac{\eta}{a_1\tau_{lf}}\int_0^t \zeta(\tau)d\tau + \frac{1}{a_1\tau_{lf}}\zeta(t). \end{aligned} \tag{22}$$
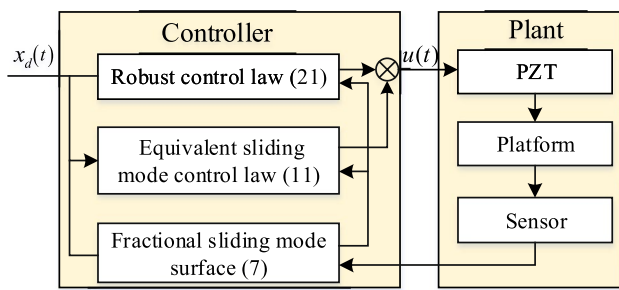
Fig. 2 Block diagram of the proposed SMCFO method

Based on the Lyapunov stability theorem, the proposed SMCFO method will make the tracking error converge to zero. That is, the PZT micro-nano platform accurately tracks the desired trajectory signal.   □

Figure 2 shows a block diagram of the proposed SMCFO method. It indicates that the designs of the robust control term and the equivalent sliding mode control law both use a fractional order sliding mode surface, which extends the freedom of the proposed controller and enhances its performance.

4 Simulation and Experimental Results

4.1 Simulation Study

To implement the controller, the parameters of the controller (22) need to be assigned, which include the time constant τ_{lf}, the order of the fractional-order operator r, the control gain η, and λ. Next, we carried out some simulation studies to determine the parameters of the controller. As shown in Fig. 3a, the time constant τ_{lf} influences the performance of the proposed controller, and its value is smaller and its tracking error is lower. However, τ_{lf} is influenced by noise and cannot be excessively small. Similarly, we adopt a variable λ to discuss the performance of the proposed controller, while keeping the other parameters unchanged. As shown in Fig. 3b, tracking error decreases as the parameter increases. Then, by varying r while keeping the other three parameters invariant, the tracking error is as shown in Fig. 3c. Note that, the bigger the value of r, the better is the controller performance. As shown in Fig. 3d, the higher the value of η, the smaller is the tracking error of the proposed controller. Next, we consider the above simulation results as the parameter selection criteria and attempt to select the experimental parameters.

4.2 Experimental Study

As shown in Fig. 4, we use this experimental setup to examine the performance of the proposed SMCFO method. It mainly consists of the host computer, PZT micro-nano platform (MPT-2MRL050), data acquisition (DAQ) card (PCI-1716), and integrated controller (PPC-2CR0150). The PZT micro-nano platform includes the piezoelectric actuator and a built-in strain gauge sensor. The driving range of the PZT micro-nano platform is from 0 to 50 μm; and the displacement resolution of the sensor is 5 nm. During the experiment, we adopt the open-loop mode of the integrated controller, which is used as a power amplifier (its driving range is from 0 to 150 V) to drive the PZT micro-nano platform. The DAQ card produces the driving signal for the
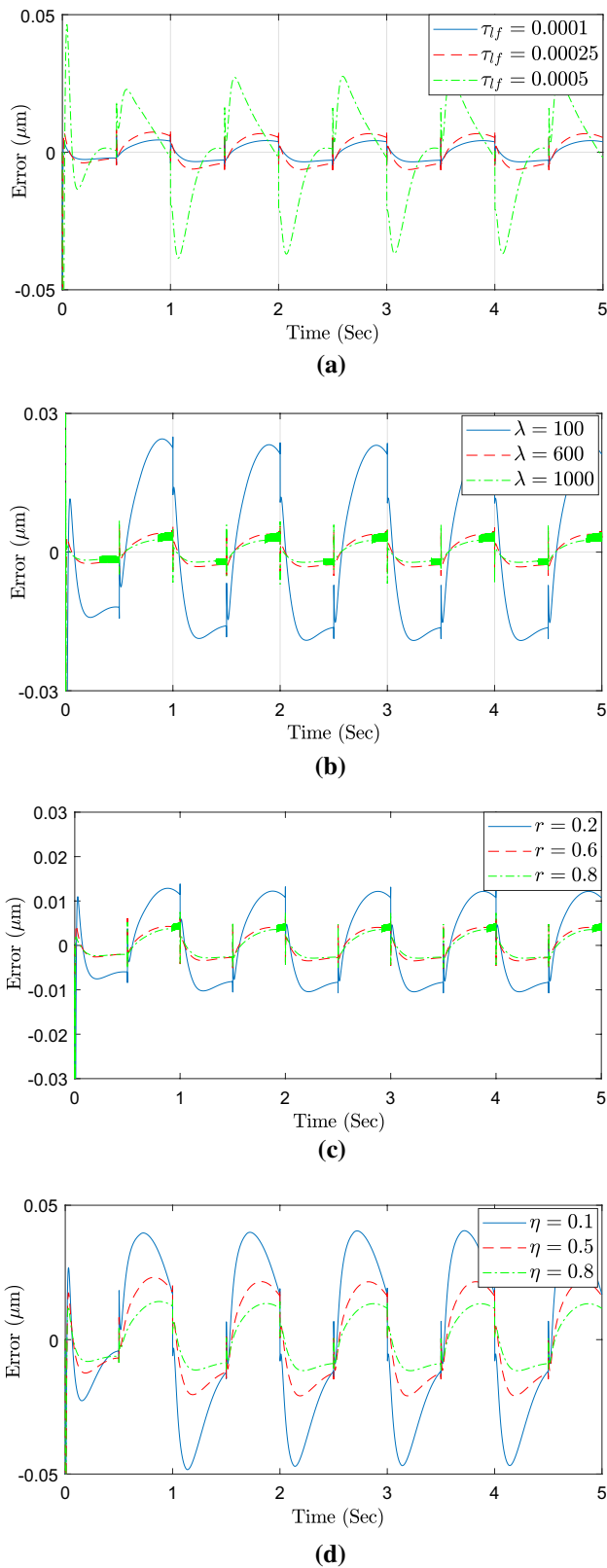
Proof For the stability proof of the control system, the Lyapunov function is defined as follows:

$$V(t) = \frac{1}{2}\zeta^2(t). \tag{23}$$

Taking the derivative of time t with respect to (23), we have the following:

$$\dot{V}(t) = \dot{\zeta}(t)\zeta(t). \tag{24}$$

Substituting (10) and (22) into (24), we can obtain

$$\begin{aligned}
\dot{V}(t) &= \zeta(t)(\hat{\phi}(t) - \phi(t) - \eta\zeta(t)) \\
&\leq \zeta(t)|\hat{\phi}(t) - \phi(t)| - \eta|\zeta(t)|^2.
\end{aligned} \tag{25}$$

According to (16), we obtain

$$\hat{\phi}(t) - \phi(t) = g_{lf}(t) * \phi(t) - \phi(t). \tag{26}$$

Then, taking the Laplace transform of (26), the following is derived:

$$\begin{aligned}
\hat{\Phi}(s) - \Phi(s) &= G_{lf}(s)\Phi(s) - \Phi(s) \\
&= (G_{lf}(s) - 1)\Phi(s).
\end{aligned} \tag{27}$$

Because $G_{lf}(s)$ is a low-pass filter, it possesses the unity gain and zero phase shift for the frequency spectrum of the disturbance $\phi(t)$. Therefore, based on (27), the following is derived:

$$\hat{\Phi}(s) - \Phi(s) = 0. \tag{28}$$

Taking the inverse Laplace transform of (28), the following is obtained:

$$\hat{\phi}(t) - \phi(t) = 0. \tag{29}$$

Therefore, the (25) is rewritten as follows:

$$\dot{V}(t) \leq -\eta|\zeta(t)|^2 \leq 0. \tag{30}$$

From the above, it is clear that the Lyapunov function (23) is positive definite, and its time derivative is negative definite.

Fig. 3 Some simulation results of the proposed SMCFO method. **a** Error versus the parameter τ_{lf}. **b** Error versus the parameter λ. **c** Error versus the parameter r. **d** Error versus the parameter η
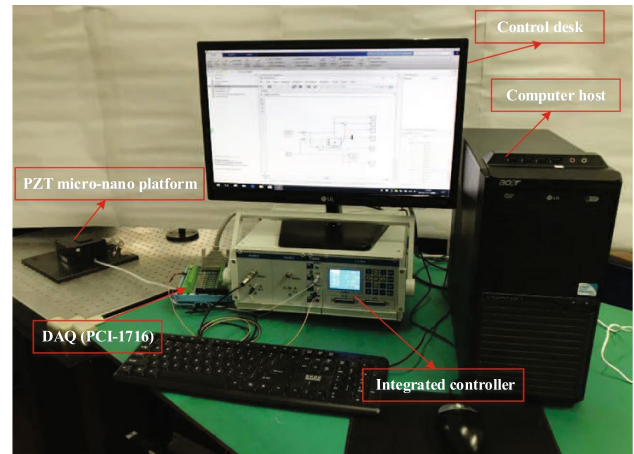

Fig. 4 Picture of the experimental setup

power amplifier and collects the output displacement signal of the sensor. The control algorithm is carried out using the host computer with the MATLAB software (Real-Time Windows Target toolbox). Figure 5 show a block diagram of the experimental setup, which illustrates the experimental process more clearly.

To test the performance of the proposed SMCFO method, we apply a 1 Hz sine wave signal as the reference signal, the travel range of which is 36 μm. The parameters of the SMCFO method are set as $\tau_{lf} = 0.0001$, $\lambda = 600$, $r = 0.6$, and $\eta = 0.8$. For comparison, the traditional SMC method is implemented. The experimental results are shown in Fig. 6. The figure indicates that the MAXE and RMSE of the proposed SMCFO method are 0.0859 μm and 0.0123 μm, respectively, whereas such values of the traditional SMC method are 0.0962 μm and 0.0166 μm. Based on these experimental results, the superiority of the SMCFO method to a traditional SMC is noticeable. In addition, when the frequency of the desired trajectory signal is 1 Hz, the obtained Duhem model can accurately capture the hysteresis of the PZT micro-nano platform. The unmodeled dynamic of the platform without a load has little influence on the entire control system. However, the performance of the proposed controller is also superior to that of the traditional SMC method.

Next, a sine wave signal of 50 Hz and an amplitude of 36 μm is used as the reference signal to execute the comparison experiments. The resulting graphs for the SMCFO
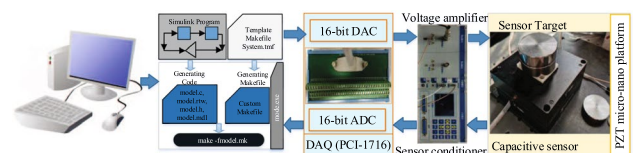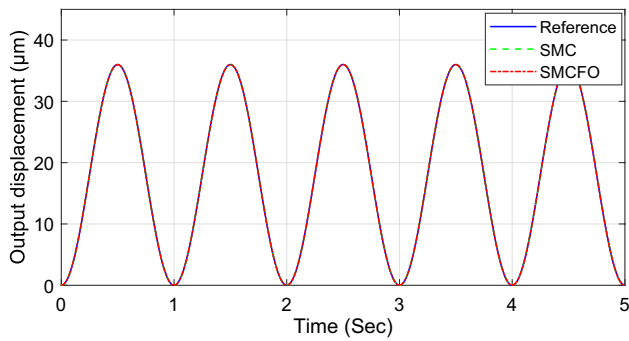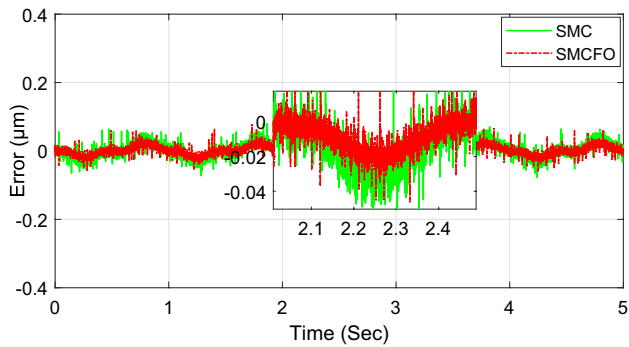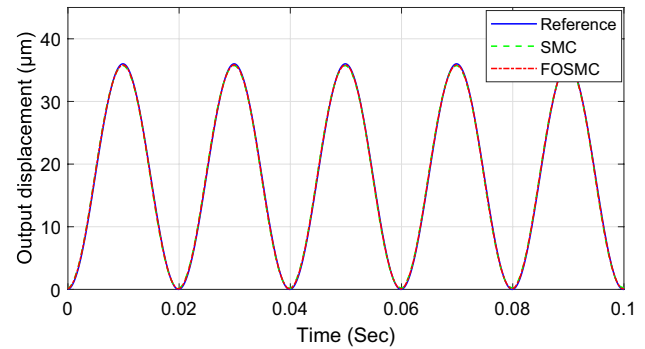

Fig. 5 Block diagram of the experimental setup

Fig. 6 Tracking experimental results of the SMC and the proposed SMCFO approach with 1 Hz reference trajectory. **a** Tracking curves. **b** Tracking error
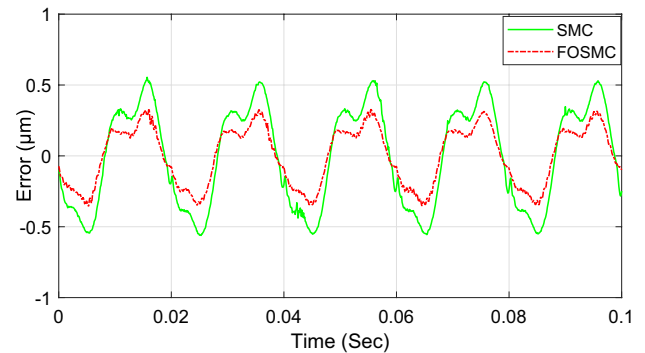

Fig. 7 Tracking experimental results of the SMC and the proposed SMCFO approach with 50 Hz reference trajectory. **a** Tracking curves. **b** Tracking error

and the traditional SMC method are plotted in Fig. 7. The MAXE and RMSE of the proposed SMCFO method are 0.3558 μm and 0.2078 μm, respectively, which are 35.8% and 41.3% less than those of the traditional SMC.

The third set point is the complex trajectory signal, and Fig. 8 plots the experimental tracking results. It can be seen that the tracking error of the proposed SMCFO method is less than that of the traditional SMC method. This further proves that the proposed SMCFO method achieves a better performance in suppressing the hysteresis of the PZT micro-nano platform, in comparison with the traditional SMC method. To avoid experiment contingency, the experiment was repeated by five times. Fig. 9 plots the RMSE bar of the PZT micro-nano platform based on the proposed SMCFO method. From Fig. 9, it can be seen that the residual error is small, which reveals that the proposed controller has an excellent and steady tracking performance. However, owing to the influence of the bandwidth (which is approximately 66.7 Hz based on testing) of the proposed controller, the tracking errors increase with the reference signal frequency. However, the proposed controller also shows better tracking performance than the traditional SMC method.

Finally, tracking experiments based on the proposed controller are implemented by mounting the loads on the platform to validate the robustness of the developed controller against the external perturbation. When the reference trajectory is a 1-Hz sine wave signal, we mount some weights of 0, 100, 200, 300, 400, and 500 g weights onto the PZT micro-nano platform to carry out the motion tracking experiments with the proposed SMCFO method. We then implement three other groups of tracking experiments with different frequencies (15, 25, and 50 Hz) as reference signals. The experimental results are shown in Fig. 10. It is clear that the MAXE rate, RMSE, and mean error (ME) of the proposed SMCFO method only exhibit slight changes under different weights. For example, when the tracking of a 50-Hz sine wave signal with an amplitude of 36 μm is examined, the fluctuation ranges of the MAXE rate, RMSE, and ME based on the SMCFO method are ± 0.015%, ± 0.003 μm, and ± 0.009 μm, respectively. This indicates the excellent robustness of the developed SMCFO method.

5 Conclusions

In this paper, a novel SMCFO method with a fractional-order operator is proposed to eliminate the hysteresis of the PZT micro-nano platform and achieve a high-precision
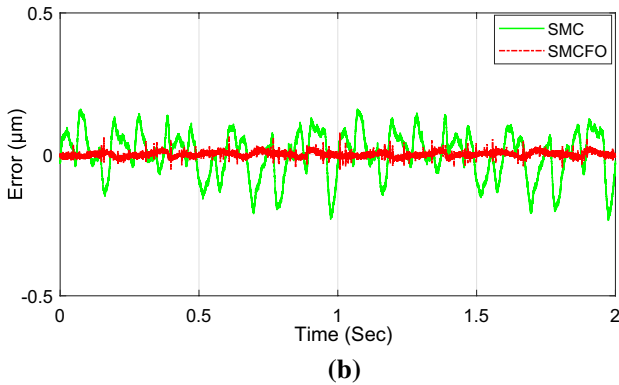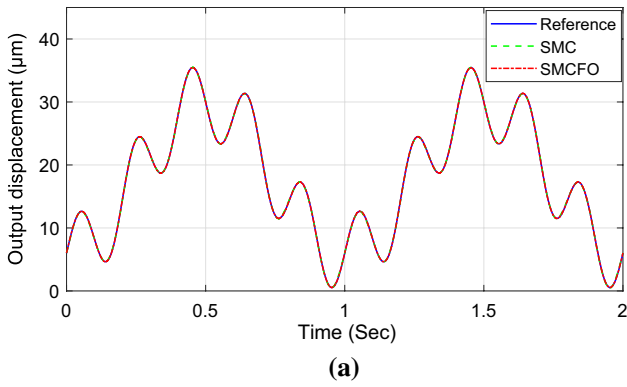
(a)

(b)

Fig. 8 Tracking experimental results of the SMC and the proposed SMCFO approach with the complex reference trajectory. **a** Tracking curves. **b** Tracking error
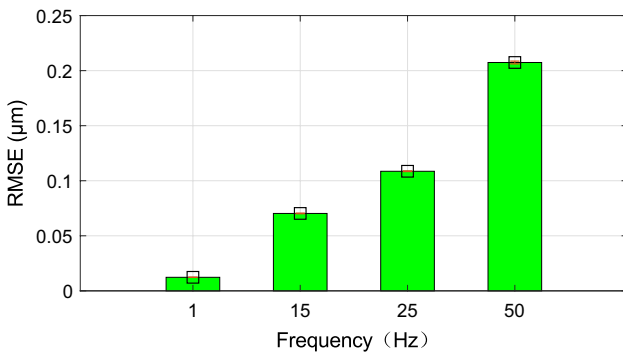

Fig. 9 Tracking experimental results of the proposed SMCFO approach with the different frequencies reference trajectory

(a)

(b)

(c)

Fig. 10 Tracking experimental results of the SMCFO approach with the different weights. **a** MAXE rate. **b** RMSE. **c** ME

tracking control. Unlike the existing sliding mode surface design method, a fractional-order operator is introduced, which increases the degrees of the proposed sliding mode surface. In addition, a continuous control term based on the low-pass filter is used to design the sliding mode controller and replace the traditional signum function. This offers the advantage of being essentially chattering-free. The s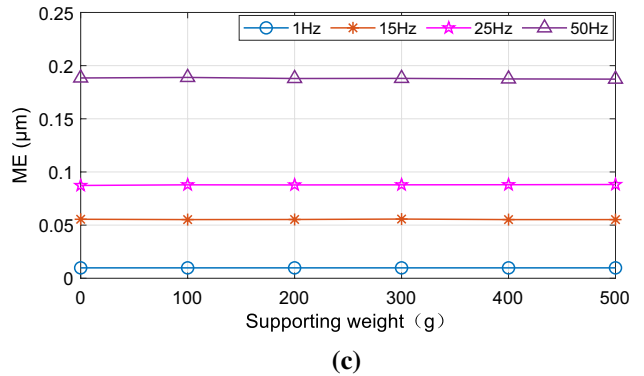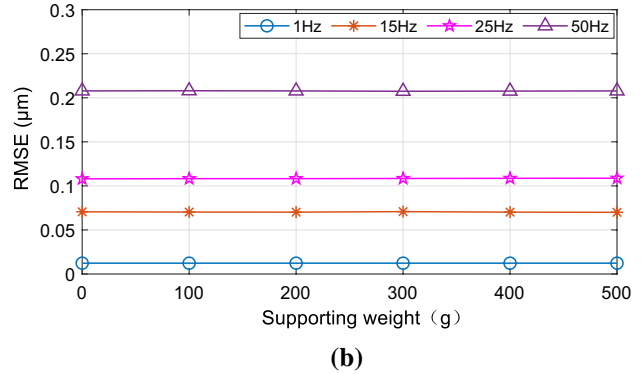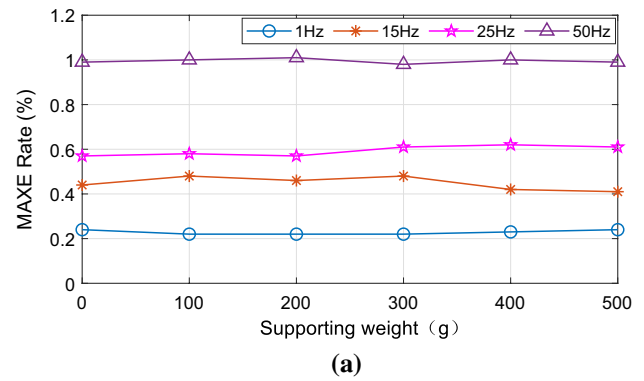tability of the proposed SMCFO method is demonstrated using the Lyapunov stability analysis in theory. The effectiveness of the proposed SMCFO method is tested through simulations and experiments on the PZT micro-nano platform. The results show that the developed SMCFO method achieves better performance than the traditional SMC method.

References

1. Leang, K., Zou, Q., & Devasia, S. (2009). Feedforward control of piezoactuators in atomic force microscope systems. *IEEE Control Systems Magazine*, *29*(1), 70–82.

2. Ho, S., & Jan, S. (2015). A piezoelectric motor for precision positioning applications. *Precision Engineering*, *43*, 285–293.

3. Salapaka, S. M., & Salapaka, M. V. (2008). Scanning probe microscopy. *IEEE Control Systems Magazine*, *28*(2), 65–83.

4. Stakvik, J., Ragazzon, M. R. P., Eielsen, A. A., & Gravdahl, J. T. (2015). On implementation of the Preisach model identification and inversion for hysteresis compensation, modeling. *Identification and Control (MIC)*, *36*(3), 133–142.

5. Li, Z., Shan, J., & Gabbert, U. (2019). Inverse compensator for a simplified discrete preisach model using model-order reduction approach. *IEEE Transactions on Industrial Electronics*, *66*(8), 6170–6178.

6. Bobbio, S., Miano, G., Serpico, C., & Visone, C. (1997). Models of magnetic hysteresis based on play and stop hysterons. *IEEE Transactions on Magnetics*, *33*(6), 4417–4426.

7. Li, Z., Shan, J., & Gabbert, U. (2018). Inverse compensation of hysteresis using Krasnoselskii–Pokrovskii model. *IEEE/ASME Transactions on Mechatronics*, *23*(2), 966–971.

8. Xu, R., Tian, D., & Wang, Z. (2020). Adaptive tracking control for the piezoelectric actuated stage using the Krasnoselskii–Pokrovskii operator. *Micromachines*, *11*(5), 1–13.

9. Xu, R., & Zhou, M. (2017). Elman neural network-based identification of Krasnosel'skii–Pokrovskii model for magnetic shape memory alloys actuator. *IEEE Transactions on Magnetics*, *11*(5), 2002004.

10. Habineza, D., Rakotondrabe, M., & Le Gorrec, Y. (2015). Bouc–Wen modeling and feedforward control of multivariable hysteresis in piezoelectric systems: Application to a 3-DoF piezotube scanner. *IEEE Transactions on Control Systems Technology*, *23*(5), 1797–1806.

11. Wang, G., Chen, G., & Bai, F. (2015). Modeling and identification of asymmetric Bouc–Wen hysteresis for piezoelectric actuator via a novel differential evolution algorithm. *Sensors and Actuators A Physical*, *235*, 105–118.

12. Su, C.-Y., Stepanenko, Y., Svoboda, J., & Leung, T. P. (2000). Robust adaptive control of a class of nonlinear systems with unknown backlash-like hysteresis. *IEEE Transactions on Automatic Control*, *45*(12), 2427–2432.

13. Zhou, M., Yang, P., Wang, J., & Gao, W. (2016). Adaptive sliding mode control based on duhem model for piezoelectric actuators. *IETE Technical Review*, *33*(5), 557–568.

14. Xu, R., Zhang, X., Guo, H., & Zhou, M. (2018). Sliding mode tracking control with perturbation estimation for hysteresis nonlinearity of piezo-actuated stages. *IEEE Access*, *6*, 30617–30629.

15. Liang, C., Wang, F., Tian, Y., Zhao, X. Y., & Zhang, D. W. (2017). Grasping force hysteresis compensation of a piezoelectric-actuated wire clamp with a modified inverse Prandtl–Ishlinskii model. *Review of Scientific Instruments*, *88*(11), 115101.

16. Feng, Z., Ling, J., Ming, M., & Xiao, X. (2018). A model-data integrated iterative learning controller for flexible tracking with application to a piezo nanopositioner. *Transactions of the Institute of Measurement and Control*, *40*(10), 3201–3210.

17. Kim, B., Washington, G. N., & Yoon, H. S. (2012). Hysteresis-reduced dynamic displacement control of piezoceramic stack actuators using model predictive sliding mode control. *Smart Materials and Structures*, *21*(5), 055018.

18. Ming, M., Ling, J., Feng, Z., & Xiao, X. (2018). A model prediction control design for inverse multiplicative structure based feedforward hysteresis compensation of a piezo nanopositioning stage. *International Journal of Precision Engineering and Manufacturing*, *19*(11), 1699–1708.

19. Cheng, L., Liu, W., Hou, Z. G., Yu, J., & Tan, M. (2015). Neural-network-based nonlinear model predictive control for piezoelectric actuators. *IEEE Transactions on Industrial Electronics*, *62*(12), 7717–7727.

20. Ling, J., Feng, Z., Ming, M., & Xiao, X. (2018). Damping controller design for nanopositioners: A hybrid reference model matching and virtual reference feedback tuning approach. *International Journal of Precision Engineering and Manufacturing*, *19*(1), 13–22.

21. Li, Y., & Xu, Q. (2012). Design and robust repetitive control of a new parallel-kinematic XY piezostage for micro/nanomanipulation. *IEEE/ASME Transactions on Mechatronics*, *17*(6), 1120–1132.

22. Li, C. X., Gu, G. Y., Yang, M. J., & Zhu, L. M. (2015). High-speed tracking of a nanopositioning stage using modified repetitive control. *IEEE Transactions on Automation Science and Engineering*, *14*(3), 1467–1477.

23. Xu, R., & Zhou, M. (2017). Sliding mode control with sigmoid function for the motion tracking control of the piezo-actuated stages. *Electronics Letters*, *53*(2), 75–77.

24. Xu, Q. (2017). Precision motion control of piezoelectric nanopositioning stage with chattering-free adaptive sliding mode control. *IEEE Transactions on Automation Science and Engineering*, *14*(1), 238–248.

25. Chen, X., & Hisayama, T. (2008). Adaptive sliding-mode position control for piezo-actuated stage. *IEEE Transactions on Industrial Electronics*, *55*(11), 3927–3934.

26. Li, Y., & Xu, Q. (2010). Adaptive sliding mode control with perturbation estimation and PID sliding surface for motion tracking of a piezo-driven micromanipulator. *IEEE Transactions on Control Systems Technology*, *18*(4), 798–810.

27. Shieh, H.-J., & Huang, P.-K. (2007). Precise tracking of a piezoelectric positioning stage via a filtering-type sliding-surface control with chattering alleviation. *IET Control Theory and Applications*, *1*(3), 586–594.

28. Xu, Q. (2017). Continuous integral terminal third-order sliding mode motion control for piezoelectric nanopositioning system. *IEEE/ASME Transactions on Mechatronics*, *22*(4), 1828–1838.

29. Emelyanov, S. V., Korovin, S. K., & Levant, A. (1996). High-order sliding modes in control systems. *Mathematical and Computer Modelling*, *7*(3), 294–318.

30. Ren, B., Zhong, Q., & Chen, J. (2015). Robust control for a class of nonaffine nonlinear systems based on the uncertainty and disturbance estimator. *IEEE Transactions on Industrial Electronics*, *62*(9), 5881–5888.

31. Zhu, Y., & Zhu, S. (2014). Adaptive sliding mode control based on uncertainty and disturbance estimator. *Mathematical Problems in Engineering*, *2014*(982101), 1–10.

32. Wang, G., & Chen, G. (2017). Identification of piezoelectric hysteresis by a novel Duhem model based neural network. *Sensors and Actuators A Physical*, *264*, 282–288.

33. Dong, R., Tan, Y., & Xie, Y. (2016). Identification of micropositioning stage with piezoelectric actuators. *Mechanical Systems and Signal Processing*, *75*, 618–630.

Rui Xu received the Ph.D. degree in control theory and control engineering with the Department of Control Science and Engineering, Jilin University, Changchun, China, in 2019. From Sep. 2018 to Sep. 2019, he was an exchange PhD student with the Department of Electrical and Computer Engineering, Michigan State University, East Lansing, USA. Since 2020, he has been with the Key Laboratory of Airborne Optical Imaging and Measurement, Changchun Institute of Optics, Fine Mechanics and Physics, Chinese Academy of Sciences, Changchun, China. His current research interests include Micro-nano drive control, motion control theory and optical imaging.

Wei Pan received the B.S. and M.S. degrees in automation from the Nanchang University and Jilin University, China, in 2017 and 2020, respectively. Her research interests include micro/nano drive and control technology.

Zhongshi Wang received the B.Eng. degree from the College of Automation, Haerbin Engineering University, China, in 2011, and the M.Eng. degree from the College of Automation, Haerbin Engineering University, China, in 2014. He is currently an assistant researcher in the Key Laboratory of Airborne Optical Imaging and Measurement (AOIM), Changchun Institute of Optics, Fine Mechanics and Physics (CIOMP), and pursuing the Ph.D. degree in mechanical and electronic engineering, from University of Chinese Academy of Sciences. His research interests include disturbance observer and nonlinear control system.

Dapeng Tian received the B.E. degrees from Beijing Institute of Technology, Beijing, China, in 2007 and in 2012, respectively. He was then directly recommended to study at the Beijing University of Aeronautics and Astronautics (Beihang University), Beijing, where he received the Ph.D. degree in 2012. From 2009 to 2012, he was a Co-researcher with the Advanced Research Center, Keio University, Yokohama, Japan. Since 2012, he has been with the Key Laboratory of Airborne Optical Imaging and Measurement, Changchun Institute of Optics, Fine Mechanics and Physics, Chinese Academy of Sciences, Changchun, China. He achieved the 2017's outstanding science and technology achievement prize of the Chinese Academy of Sciences and 2018's state science and technology award in China. His current research interests include motion control theory and engineering, optical imaging, and bilateral control.